

**Enhanced hydrophilic and antibacterial activity against *E. coli* of PVDF ultrafiltration
membrane blended with Ag₃PO₄/TiO₂ nanocomposite**

Xiaoting Hong ^{a,*}, Yumei Zhou ^b, Zhuoliang Ye ^c, Haifeng Zhuang ^a, Wanpeng Liu ^a, K.S. Hui ^d, Zhi
Zeng ^b

^a School of Civil Engineering and Architecture, Zhejiang University of Science and Technology; Key
Laboratory of Recycling and Eco-treatment of Waste Biomass of Zhejiang Province, Hangzhou 310023,
China

^b School of Chemistry & Environment, South China Normal University, Guangzhou 510006, China

^c School of Chemical Engineering, Fuzhou University, Fuzhou, Fujian 350116, P. R. China

^d School of Mathematics, Faculty of Science, University of East Anglia, Norwich, NR4 7TJ, United
Kingdom

Corresponding author. Tel.: +86 (0571) 81315186, Fax +86 (0571) 81315186.

E-mail address: hanren.xiaoting@gmail.com (X.T. Hong), yezl@fzu.edu.cn (Z. Ye).

Abstract:

$\text{Ag}_3\text{PO}_4/\text{TiO}_2$ nanocomposite was fabricated by an in-situ precipitation method and then blended into poly(vinylidene fluoride) (PVDF) casting solution to prepare the ultrafiltration membrane via wet phase inversion technique. The water flux and bovine serum albumin (BSA) rejection rate of membrane were investigated meanwhile the ultrafiltration membrane morphologies and structural properties were analyzed using scanning electron microscope (SEM) and X-ray diffraction (XRD). Compared with the control membrane, the permeate performance of blended membranes was improved while possessing a steady BSA retention due to enhanced hydrophobicity. Mechanical tests revealed that the modified membranes exhibited a larger tensile strength and breakage elongation. SEM images and the halo zone testing were employed to assess the antibacterial performances of the nanocomposite membranes against *E. coli*. The antibacterial tests confirmed that the modified membranes showed an effective antibacterial property against *E. coli*.

Keywords: Phase-inversion; PVDF ultrafiltration membrane; $\text{Ag}_3\text{PO}_4/\text{TiO}_2$ nanocomposite; hydrophilic and antibacterial

1. Introduction

As a increasing global demand for water security and more stringent environmental requirements, membrane treatment processes play a significant role in water and wastewater treatment and maintain steady increase over the past few years ascribed to its advantages and specific characteristics such as compactness, high efficiency, ease operation, and low energy consumption [1-3]. In particular, polyvinylidene fluoride (PVDF) membrane is broadly employed for the processes of pervaporation, reverse osmosis, microfiltration and ultrafiltration ascribed to its extraordinary thermal, chemical stability, high mechanical strength, and inertness derived from its fluorinated structure [4, 5]. Nevertheless, membrane fouling, which results in unpredictably decreased life span and severe damage of the membranes, is still one of the important threats for PVDF membrane treatment technology because of its intrinsic hydrophobic nature and low surface energy property [1, 6, 7].

In order to make PVDF membranes less prone to irreversible fouling, lots of efforts have been devoted to improve membrane antifouling property and permeability in addition to the optimization of cleaning methods and operating conditions [8, 9], including material modification, polymer blend and surface modification [10, 11]. Among them, blending modification by incorporation inorganic nanomaterials to synthesize nanoparticle functionalized membranes has become a great interest for manufactures and researchers [12-14]. The blended membranes normally achieve the desired enhancement of separation properties since the resultant nanocomposite membranes simultaneously possess comprehensive characteristics of the blended nanomaterials and matrix membrane materials. Currently, many researchers have focused on Al_2O_3 , SiO_2 , and TiO_2 nanoparticles as blending materials for PVDF surface modification [15-19]. Among them, TiO_2 nanoparticles have achieved great attention due to the high hydrophilicity, excellent chemical stability, and potential antifouling abilities [20, 21, 22, 23].

A large number of studies have investigated the influences of TiO_2 blending on the enhancement of PVDF membrane properties [24]. Cao et al. reported the effects of TiO_2 nanoparticle size on the separation behavior and morphology of PVDF membrane and suggested nanosized TiO_2 with 10 nm for blending modification [25]. Damodar et al. investigated the impacts of different dosages of TiO_2 nanoparticles in the PVDF dope on their antibacterial and antifouling behaviors, and found that good hydrophilicity of membrane was established by adding low concentration of TiO_2 into the PVDF casting solution [26]. Oh et al. modified PVDF-UF membrane with TiO_2 nanoparticles and found that

the anti-fouling capability of the nanocomposite PVDF membranes was significantly improved [27]. Normally, blending TiO₂ nanoparticles greatly influenced the pore size distribution and surface hydrophilicity of the nanocomposite membrane and thus the flux and permeability of TiO₂ blended PVDF membrane was improved [28]. Compared to the unmodified PVDF membrane, incorporation of TiO₂ nanoparticles into membrane matrix could also show better antibacterial and antifouling capabilities upon UV light irradiation [28]. Bacteria are the major microorganisms which lead to severe membrane fouling and irreversibly deteriorate membrane performance. To alleviate the bacteria induced membrane fouling during membrane filtration processes, it is vitally important to ensure the membrane possessing an antibacterial property [29, 30]. Therefore, an effective strategy is usually proposed to add inorganic antibacterial agents such as silver nanoparticles or Ag-loaded nanocomposites.

In this study, an Ag-loaded TiO₂ nanocomposite (Ag₃PO₄/TiO₂) was successfully blended into casting solution to improve the antifouling behavior and surface hydrophilicity of the PVDF nanocomposite membrane via the wet phase inversion process. The surface hydrophilicity, antibacterial behaviors and mechanical strength of the as-synthesized PVDF nanocomposite membranes were expected to be substantially approved. The influence of the different dope solution composition on the structural properties and separation performances of the resultant nanocomposite membranes were comprehensively explored with respect to BSA rejection ratios, pure water flux, surface morphologies, surface hydrophilicity, tensile strength, pore size and fouling resistance. The antibacterial property of Ag₃PO₄/TiO₂ blended nanocomposite membrane was revealed by the adhesion of E. coli bacteria to membranes and halo zone testing.

2. Materials and methods

2.1 Material

All reagents were used without further purification. FR-904 PVDF was purchased from Shanghai 3F New Material Co., Ltd. It was dried at 100 °C overnight in a vacuum oven prior to use for dope solution. Commercial TiO₂ (Degussa P25, Germany), silver nitrate (99.8%), polyvinyl pyrrolidone (PVP, K-30), ethyl alcohol (99.7%), sodium chloride (99.5%), N, N-dimethyl formamide (DMF), trisodium phosphate, anhydrous disodium hydrogen phosphate, anhydrous sodium hydrogen phosphate, glutaraldehyde, isoamyl acetate were supplied by Shanghai Aladdin Bio-Chem Technology Co., Ltd.

Nutrient agar, yeast extract, and peptone were provided by Shanghai bluetech and Beijing Aoboxing Biotechnology Co. Ltd, respectively. A Millipore Milli-Q Advantage A10 system was used to produce the DI water. *E. coli* DH 5 α was provided by Sun Yat-sen University.

2.2 Preparation of Ag₃PO₄/TiO₂ nanocomposite

The immobilization of Ag₃PO₄ nanoparticles onto the TiO₂ surface was achieved by an in-situ precipitation method [31]. Firstly, 10 g TiO₂ was dispersed in 50 ml deionized water and sonicated for five minutes. Then 3 g AgNO₃ was added to the above TiO₂ suspension. Na₃PO₄ solution was prepared by dissolving 2.3 g Na₃PO₄ in 30 mL deionized water. Na₃PO₄ solution was subsequently added dropwise to the TiO₂ suspension. The mixture was continuously stirred for five hours at room temperature, finally the color of the solution changed from white to yellow. The precipitated solid product (Ag₃PO₄/TiO₂) was then filtered, washed and dried for subsequent use.

2.3 Fabrication of Ag₃PO₄/TiO₂ blended membranes

Different amounts of TiO₂ and Ag₃PO₄/TiO₂ nanocomposite were uniformly dispersed in the DMF solvent with the aid of sonication. Subsequently, PVDF and PVP were added into the suspensions with the aid of agitation for 4 h to prepare a homogeneous mixture, and then degassed at 60 °C overnight under negative pressure to remove air bubbles. All the as-synthesized nanocomposite membrane compositions were illustrated in Table 1. The dope solution was casted evenly onto a glass substrate with a casting knife gap of 250 μ m. The fresh membrane was transferred into the DI water bath at ambient temperature. A similar casting dope without any blending material was prepared as a control.

2.4 Characterization of Ag₃PO₄/TiO₂ nanocomposite

The XRD patterns were recorded using a Y-2000 diffractometer (Bruker AXS D8 Advance, Germany) with monochromatic Cu K α 1 radiation ($\lambda = 1.5406$ Å, 40 kV, 20 mA). The 2 θ angular regions between 10 and 90 ° were used to confirm the crystalline structures of TiO₂ and Ag₃PO₄/TiO₂ nanocomposite.

The morphological properties and selected area electron diffraction (SAED) were observed on a JEOL JEM-2100HR Transmission electron microscopy (TEM) equipped with an energy-dispersive X-ray (EDX) spectrometer.

2.5 Characterization of the blended membranes

2.5.1 Structural characterization

The membranes were coated with a conductive platinum film by sputter coating method under vacuum

and positioned on a metal holder to investigate the surface morphologies with a ZEISS Ultra 55 FE-SEM. The samples for a clear cross-section SEM images were prepared by a fracture of the dried membranes in liquid nitrogen and then a platinum coating. The XRD patterns were recorded in the 2 θ angular regions from 10 to 60 ° to study the crystalline structures of the nanocomposites.

2.5.2 Separation performance of membrane samples

The water flux of the nanocomposite membranes was carried out using a MSC300 ultrafiltration cup (Shanghai Mosu Science Equipment Co., Ltd.). The membrane was firstly filtered with DI water for 40 min at 0.1 MPa until the flux was steady prior to investigating the membrane retention behavior by 1 g/L BSA aqueous solution. BSA concentrations in the feed solution and the permeation were measured by a UV-Vis spectrophotometer (UV-1800, Shimadzu) at λ_{\max} of 280 nm.

The permeate flux (J_w) was calculated using Eq. (1)

$$J_w = \frac{V}{A \times \Delta t} \quad (1)$$

where V is the total volume of permeation (L), Δt was the permeation time (h), and A is the effective membrane area (m²). The whole experiments were carried out at room temperature.

The BSA rejection was determined by the ratio the BSA concentration in the feed solution and permeation according to Eq. (2)

$$R\% = \frac{C_f - C_p}{C_f} \times 100\% \quad (2)$$

where C_p and C_f were the concentrations of the permeate and the feed solution, respectively.

The membrane hydrophilicity of was characterized by the water contact angle using a contact angle instrument (SL200B, USA KINO Industry Co., Ltd.). Firstly, a drop of DI water with 5 μ L was loaded onto the outer surface of the as-synthesized membrane by a manual microliter syringe. Subsequently, the static water contact angle was measured immediately after taking the droplet image. Finally, the average value of the contact angle was obtained from the measurements of ten different points on each membrane.

The porosity of the nanocomposite membranes was determined by the dry-wet weight method reported elsewhere [32]. The porosity ε (%) of the membranes was determined according to Eq. (3)

$$\varepsilon = \frac{(W_1 - W_2) / \rho_{water}}{(W_1 - W_2) / \rho_{water} + W_2 / \rho_{PVDF}} \times 100\% \quad (3)$$

where W_1 is the weight of wet sample, W_2 is the weight of the dry sample, ρ_{water} is the density of pure water, and ρ_{PVDF} is the density of dry state membrane (kg/m^3).

A universal tensile testing machine was utilized to explore tensile strength and elongation at break of the PVDF membranes by under ambient conditions. Each membrane sample with an effective length of 100 mm were tested at a constant uniaxially stretching with a rate of 100 mm/min. An average value from ten-times testing was finally collected.

2.6 Determination of antibacterial activity

2.6.1 Halo zone test

The antibacterial activity of the nanoparticle blended membranes (P1 and P4) and the control membrane P0 were investigated qualitatively using the anti-E. coli zone of inhibition test as reported elsewhere [33]. The testing E. coli bacteria were firstly cultivated in 100 mL of a 2.5 wt % yeast-dextrose broth (consisting of 5 g/L yeast extract, 10 g/L sodium chloride, and 10 g/L peptone at a pH of 7.2) at 37 °C with shaking at 100 rpm for 24 h. The membrane samples were punched to prepare circular samples with ~ 2 mm in radius, and 100 μL of the E. coli solution (1×10^6 cfu/ml) was uniformly spread on the Luria-Bertani (LB) agar plate. The circular membrane specimens were then placed on the surface of treated LB plate and incubated at 37 °C for 24 h. The inhibition zone formed after 24 h served as an indicator for the antibacterial activity and was analyzed for growth inhibition.

2.6.2 Bacteria adhesion test

The bacterial adhesion to the surfaces of the control and modified membranes was evaluated by shake flask method. All membrane specimens were irradiated for sterilization by UV light (300W xenon lamp) for 1 h and presoaked in PBS solution prior to immersing into E. coli solution. Three pieces $2 \times 2 \text{ cm}^2$ membranes were immersed in 50 mL E. Coli solution (1×10^6 cfu/ml) in a 100 mL sterile Erlenmeyer flask at 37 °C and then shaken at 100 rpm for 4 h. Subsequently, the target membranes were drew out of the E. Coli solution and gently rinsed three times with PBS solution. Then the E. Coli cells on the membrane surfaces were quickly fixed with 2.5 % glutaraldehyde in PBS for ~ 4 h at 4 °C. After fixation, the membranes were removed from glutaraldehyde solution and rinsed by PBS buffer six times. Finally, they were suffered to dehydration by sequential washes of 30, 50, 70, 90 and 100 % ethanol for 10 min. After washing with 100 % isoamyl acetate, the membranes were critical point dried with CO_2 so as to observe the quantities and morphologies of bacteria adhered on the membrane

surfaces by SEM.

3. Results and discussion

Fig. 1 depicts the XRD patterns of pristine TiO₂ and as-synthesized Ag₃PO₄/TiO₂ nanocomposite. The TiO₂ diffraction pattern exhibits sharp peaks at 25.3 °, 37.9 °, 48.0 °, 54.3 °, 55.4 ° and 63.0 ° which correspond to (101), (004), (200), (105), (211), and (204) crystal planes, respectively, indicating a mixture of rutile and anatase phase. In the curve of Ag₃PO₄/TiO₂, there are three obvious peaks centered at 29.8 °, 33.3 °, and 36.6 ° which were in good agreement with the diffractions from the (200), (210), and (211) crystal planes of a body-centred cubic Ag₃PO₄, respectively. The results suggested that Ag₃PO₄ phase had been successfully deposited on the surfaces TiO₂ nanoparticles.

The dispersion of Ag₃PO₄ in Ag₃PO₄/TiO₂ nanocomposites was revealed by TEM measurements. It can be clearly seen from Fig. 2 that a lot of dark spots, which present Ag₃PO₄ nanoparticles possessing particle size of 2-8 nm in diameter, were highly dispersed on the surface of TiO₂ with particle diameter ranging from 16 to 50 nm. During the silver impregnation process, Ag⁺ was pre-adsorbed onto the TiO₂ surface and Ag₃PO₄ was thereafter formed due to the reaction of PO₄³⁻ ion with Ag⁺. It is noteworthy that selected area electron diffraction rings and points correspond to the TiO₂ multicrystalline phase and Ag₃PO₄ monocrystalline phase, respectively, which is consistent with the previous XRD characterizations. Both XRD patterns and TEM image of Ag₃PO₄/TiO₂ nanocomposites clearly show that the Ag₃PO₄ nanoparticles have been successfully loaded onto the surface of TiO₂ support.

Fig. 3 depicts the top-view and cross-sectional SEM images of the nanoparticle blended nanocomposite membranes (P1, P2, P4, and P5) and the control membrane (P0). As shown in Fig. 3A, the nanocomposite membranes (P1 and P2) is of flat and smooth features on the top surface which is similar to that of pristine control membrane (P0). From P2 to P5, it is obvious that the increased concentration of Ag₃PO₄/TiO₂ nanocomposites in the casting solution resulted in rougher surface with more fully developed macro pores on the top side of modified membranes.

As the casted PVDF dope solution on the glass substratum was immersed into the water bath for coagulation, a non-solvent/solvent exchange immediately occurred across the interface between the non-solvent and casting film. Therefore, the near-surface nanocomposites dispersed in solvent may serve as pore-forming agent. The repulsive forces between water and PVDF together with the fast non-solvent/solvent interchange caused an immediate PVDF precipitation at the interface.

Consequently, a typical asymmetric structure composed of well-developed macrovoids and finger-like pores connected by sponge walls in sub-layer was formed.

Fig. 4 presents the XRD patterns of PVDF–Ag₃PO₄/TiO₂ composite membranes and pristine PVDF membrane. There are two characteristic peaks of PVDF crystal at 2θ of 18.5 ° and 20.1 °, which correspond to the planes of (100) and (020). After incorporating TiO₂ and Ag₃PO₄/TiO₂ into the PVDF matrix, no characteristic peaks of TiO₂ and Ag₃PO₄/TiO₂ NPs were observed in the XRD patterns indicating a high compatibility between PVDF and blending materials from phase inversion process.

Table 2 summarizes all as-prepared membrane properties with respect to their porosity, contact angle, mechanical strength, and Breakage elongation. Normally, blending TiO₂ nanoparticles would be expected to significantly increase membrane porosity [34], but the membrane porosity was slightly affected by the blending materials of Ag₃PO₄/TiO₂ in this study as all the membranes prepared displayed reasonably high porosity ranging from between 84.67 to 85.05 %, which is in accord with the results elsewhere [35]. There is no controversy that high membrane porosity was dominantly contributed by the presence of hydrophilic PVP with high MW in dope solution regardless of the Ag₃PO₄/TiO₂ concentration due to the occurrence of solution demixing induced by PVP and enhancement of phase separation [36]. Mechanical properties are extremely important for PVDF membranes as the membranes breaking will lose separation performances. As shown in Table 2, with respect to mechanical strength and breakage elongation, all PVDF membranes incorporated with blending nanoparticles demonstrated greater mechanical strength compared to that of pristine membrane. The tensile strength and breakage elongation gradually reach a maximum of 1.98 MPa and 31.77 % when adding 0.3 wt % Ag₃PO₄/TiO₂ nanocomposite and then successively drop down as further increasing of the loadings of Ag₃PO₄/TiO₂. These results revealed that blending appropriate amount of Ag₃PO₄/TiO₂ in PVDF dope solution can enhance the mechanical properties of the resultant nanocomposite membranes which is consistent with the results elsewhere the literature [37, 38]. The variation of the membrane hydrophobicity caused by the casting mixture composition was investigated by the water contact angle measurements. When the weight ratio of Ag₃PO₄/TiO₂ was successively increased up to 1 wt. %, a gradual decreasing in membrane contact angle from 76.05 ° to 63.46 ° was observed since the surface of TiO₂ was abundant with oxygenated hydrophilic groups and therefore enhanced surface hydrophilicity.

As shown in Fig. 5, the pristine membrane exhibits a minimum permeate water flux of 47.15

L/m²·h and a maximum BSA rejection of 91.1 %. As the addition of TiO₂ and Ag₃PO₄/TiO₂, a remarkable improvement in permeate water flux from 57.35 to 103.72 L/m²·h was observed for the modified membranes, whereas a plateaus of BSA rejection around 83.5 % was maintained from P1 to P4 membranes until a sudden drop occurred for P5 samples. Apparently, the trend of an enhancement in water flux was complied with that of the surface hydrophilicity and water contact angle. It is universally acknowledged that an improvement in surface hydrophilicity of the nanoparticle blended nanocomposite membranes have a favorable effect on the water flux via attracting water molecules inside the modified PVDF membrane matrix and therefore facilitating their permeation across the blended membrane.

The antibacterial property of the Ag₃PO₄/TiO₂ modified membranes against *Escherichia coli* was characterized using the halo testing. Ag₃PO₄ nanoparticle has been found to be a significant antibacterial material due to slow-released silver ions which could attach to the cell membrane and then interact with the DNA or protein macromolecules in the cell to interfere or impede vital metabolic processes. As shown in Fig. 6a, it is noticeably found that P0 and P1 membranes has no inhibitive ability on the *E. coli* bacterial owing to the absence of the zone of inhibition. In contrast, a remarkable zone of inhibition without bacterial growth was observed surrounding the P2 membrane. A zone width is of ~ 2 mm clearly indicated P2 membrane had a promising antibacterial activity against *E. coli* and Ag₃PO₄/TiO₂ blending was able to improve the antifouling behavior of the modified PVDF nanocomposite membranes.

The bacterial colonies derived membrane fouling could be induced by the bacteria accumulation and adhesion on the membrane surface [39]. To investigate the *E. coli* adhesion on membranes, SEM was employed to study the quantities and morphology of cells on surface of the membranes. As shown in Fig. 6b, Ag₃PO₄/TiO₂ blended P4 membrane were found to have much less rod-shaped bacterial adherence to the surfaces compared to P0 and P1 membranes. Moreover, the *E. coli* on P4 membrane displayed an obviously deformed shape. The *E. coli* attachment results indicate that P4 membrane had a better anti-adhesive activity against *E. coli* owing to the slow-released Ag⁺ and expectedly had a greater potential in antifouling.

4. Conclusions

Hydrophilic and antibacterial membranes were successfully synthesized with wet phase-inversion

method by blending $\text{Ag}_3\text{PO}_4/\text{TiO}_2$ nanocomposite. Results revealed that water flux was dramatically increased with the addition of $\text{Ag}_3\text{PO}_4/\text{TiO}_2$ in dope solution. P4 membrane doped with 0.5 wt. % $\text{Ag}_3\text{PO}_4/\text{TiO}_2$ exhibits an enhanced permeate water flux of $80.41 \text{ L/m}^2\cdot\text{h}$ while high BSA rejection remains nearly unchanged due to synchronously increased hydrophilicity. FE-SEM images indicated that the degree of *E. coli* cells adhesion to the membrane surface was markedly reduced with blending $\text{Ag}_3\text{PO}_4/\text{TiO}_2$. Meanwhile, the halo zone tests also implied that P4 membrane had an obvious antibacterial activity against *E. coli*. Moreover, P4 membrane has a tensile strength of 1.80 MPa and 30.33 % elongation implying its potential application as an ultrafiltration membrane. In conclusion, $\text{Ag}_3\text{PO}_4/\text{TiO}_2$ blended PVDF nanocomposite membrane is of excellent separation performance while possessing a good antibacterial behavior and a high fouling resistance.

Acknowledgements

Financial support for this work was provided by the National Nature Science Foundation of China (21203067), and Zhejiang University of Science and Technology youth talent cultivation plan.

References

- [1] H.K. Oh, J.Y. Eom, S.H. Kang, B.G. Lee, H.C. Yoo, B.O. Lee, A study on enhancing physical cleaning effectiveness in microfiltration membrane system, *Desalin. Water Treat.*, 54 (2015) 3596-3602.
- [2] A. Ali, P. Aimar, E. Drioli, Effect of module design and flow patterns on performance of membrane distillation process, *Chem. Eng. J.*, 277 (2015) 368-377.
- [3] L. Francis, N. Ghaffour, A.S. Alsaadi, S.P. Nunes, G.L. Amy, PVDF hollow fiber and nanofiber membranes for fresh water reclamation using membrane distillation, *Journal of Materials Science*, 49 (2014) 2045-2053.
- [4] A.W. Qin, X. Li, X.Z. Zhao, D.P. Liu, C.J. He, Preparation and characterization of nano-chitin whisker reinforced PVDF membrane with excellent antifouling property, *J. Membr. Sci.*, 480 (2015) 1-10.
- [5] W. Li, H. Li, Y.-M. Zhang, Preparation and investigation of PVDF/PMMA/ TiO_2 composite film, *Journal of Materials Science*, 44 (2009) 2977-2984.
- [6] Y.C. Woo, J.J. Lee, L.D. Tijing, H.K. Shon, M.W. Yao, H.S. Kim, Characteristics of membrane

fouling by consecutive chemical cleaning in pressurized ultrafiltration as pre-treatment of seawater desalination, *Desalination*, 369 (2015) 51-61.

[7] T. Bohli, A. Ouederni, N. Fiol, I. Villaescusa, Evaluation of an activated carbon from olive stones used as an adsorbent for heavy metal removal from aqueous phases, *Comptes Rendus Chimie*, 18 (2015) 88-99.

[8] X.S. Yi, S.L. Yu, W.X. Shi, N. Sun, L.M. Jin, S. Wang, B. Zhang, C. Ma, L.P. Sun, The influence of important factors on ultrafiltration of oil/water emulsion using PVDF membrane modified by nano-sized $\text{TiO}_2/\text{Al}_2\text{O}_3$, *Desalination*, 281 (2011) 179-184.

[9] M.F. Rabuni, N.M. Nik Sulaiman, N. Awanis Hashim, A systematic assessment method for the investigation of the PVDF membrane stability, *Desalin. Water Treat.*, 57 (2016) 1-12.

[10] N.A. Hashim, F. Liu, M.R.M. Abed, K. Li, Chemistry in spinning solutions: Surface modification of PVDF membranes during phase inversion, *J. Membr. Sci.*, 415 (2012) 399-411.

[11] S. Wongchitphimon, R. Wang, R. Jiratananon, Surface modification of polyvinylidene fluoride-co-hexafluoropropylene (PVDF-HFP) hollow fiber membrane for membrane gas absorption, *J. Membr. Sci.*, 381 (2011) 183-191.

[12] M. Safarpour, A. Khataee, V. Vatanpour, Effect of reduced graphene oxide/ TiO_2 nanocomposite with different molar ratios on the performance of PVDF ultrafiltration membranes, *Separation and Purification Technology*, 140 (2015) 32-42.

[13] J.H. Li, B.F. Yan, X.S. Shao, S.S. Wang, H.Y. Tian, Q.Q. Zhang, Influence of Ag/TiO_2 nanoparticle on the surface hydrophilicity and visible-light response activity of polyvinylidene fluoride membrane, *Appl. Surf. Sci.*, 324 (2015) 82-89.

[14] S. Liang, K. Xiao, Y.H. Mo, X. Huang, A novel ZnO nanoparticle blended polyvinylidene fluoride membrane for anti-irreversible fouling, *J. Membr. Sci.*, 394 (2012) 184-192.

[15] F. Liu, M.R.M. Abed, K. Li, Preparation and characterization of poly(vinylidene fluoride) (PVDF) based ultrafiltration membranes using nano $\gamma\text{-Al}_2\text{O}_3$, *J. Membr. Sci.*, 366 (2011) 97-103.

[16] X.S. Yi, W.X. Shi, S.L. Yu, C. Ma, N. Sun, S. Wang, L.M. Jin, L.P. Sun, Optimization of complex conditions by response surface methodology for APAM-oil/water emulsion removal from aqua solutions using nano-sized $\text{TiO}_2/\text{Al}_2\text{O}_3$ PVDF ultrafiltration membrane, *J. Hazard. Mater.*, 193 (2011) 37-44.

[17] H.Q. Liang, Q.Y. Wu, L.S. Wan, X.J. Huang, Z.K. Xu, Thermally induced phase separation

followed by in situ sol-gel process: A novel method for PVDF/SiO₂ hybrid membranes, *J. Membr. Sci.*, 465 (2014) 56-67.

[18] J. Dai, K. Xiao, H. Dong, W. Liao, X. Tang, Z. Zhang, S. Cai, Preparation of Al₂O₃/PU/PVDF composite membrane and performance comparison with PVDF membrane, PU/PVDF blending membrane, and Al₂O₃/PVDF hybrid membrane, *Desalin. Water Treat.*, 57 (2016) 487-494.

[19] H. Dong, K. Xiao, X. Li, Z. Wang, S. Guo, Preparation of PVDF/Al₂O₃ hybrid membrane via alkaline modification and chemical coupling process, *Desalin. Water Treat.*, 51 (2013) 3800-3809.

[20] J.P. Mericq, J. Mendret, S. Brosillon, C. Faur, High performance PVDF-TiO₂ membranes for water treatment, *Chem. Eng. Sci.*, 123 (2015) 283-291.

[21] A.W. Qin, X. Li, X.Z. Zhao, D.P. Liu, C.J. He, Engineering a Highly Hydrophilic PVDF Membrane via Binding TiO₂ Nanoparticles and a PVA Layer onto a Membrane Surface, *ACS Appl. Mater. Interfaces*, 7 (2015) 8427-8436.

[22] S. Qiu, X. Huang, S. Xu, F. Ma, The Antibacterial Activity of Ceramsite Coated by Silver Nanoparticles in Micropore, *Applied Biochemistry and Biotechnology*, 176 (2015) 267-276.

[23] M. Tavakolmoghadam, T. Mohammadi, M. Hemmati, F. Naeimpour, Surface modification of PVDF membranes by sputtered TiO₂: fouling reduction potential in membrane bioreactors, *Desalin. Water Treat.*, 57 (2016) 3328-3338.

[24] Y. Ma, F. Shi, J. Ma, Effect of TiO₂ contents on the crystallization kinetics of PVDF in PVDF-diluent-TiO₂ blends, *Desalin. Water Treat.*, 56 (2015) 752-759.

[25] X.C. Cao, J. Ma, X.H. Shi, Z.J. Ren, Effect of TiO₂ nanoparticle size on the performance of PVDF membrane, *Appl. Surf. Sci.*, 253 (2006) 2003-2010.

[26] R.A. Damodar, S.J. You, H.H. Chou, Study the self cleaning, antibacterial and photocatalytic properties of TiO₂ entrapped PVDF membranes, *J. Hazard. Mater.*, 172 (2009) 1321-1328.

[27] S.J. Oh, N. Kim, Y.T. Lee, Preparation and characterization of PVDF/TiO₂ organic-inorganic composite membranes for fouling resistance improvement, *J. Membr. Sci.*, 345 (2009) 13-20.

[28] M.T. Moghadam, G. Lesage, T. Mohammadi, J.P. Mericq, J. Mendret, M. Heran, C. Faur, S. Brosillon, M. Hemmati, F. Naeimpour, Improved antifouling properties of TiO₂/PVDF nanocomposite membranes in UV-coupled ultrafiltration, *J. Appl. Polym. Sci.*, 132 (2015) 15.

[29] X. Li, R.Z. Pang, J.S. Li, X.Y. Sun, J.Y. Shen, W.Q. Han, L.J. Wang, In situ formation of Ag nanoparticles in PVDF ultrafiltration membrane to mitigate organic and bacterial fouling, *Desalination*,

324 (2013) 48-56.

[30] Y. Sui, Z. Wang, C. Gao, A new synthetical process of PVDF derivatives via atom transfer radical graft polymerizations and its application in fabrication of antifouling and antibacterial PVDF ultrafiltration membranes, *Desalin. Water Treat.*, 52 (2014) 6377-6388.

[31] W.F. Yao, B. Zhang, C.P. Huang, C. Ma, X.L. Song, Q.J. Xu, Synthesis and characterization of high efficiency and stable $\text{Ag}_3\text{PO}_4/\text{TiO}_2$ visible light photocatalyst for the degradation of methylene blue and rhodamine B solutions, *J. Mater. Chem.*, 22 (2012) 4050-4055.

[32] C.J. Liao, P. Yu, J.Q. Zhao, L.M. Wang, Y.B. Luo, Preparation and characterization of NaY/PVDF hybrid ultrafiltration membranes containing silver ions as antibacterial materials, *Desalination*, 272 (2011) 59-65.

[33] M.Y. Zhang, K.S. Zhang, B. De Gusseme, W. Verstraete, Biogenic silver nanoparticles (bio-Ag-0) decrease biofouling of bio-Ag-0/PES nanocomposite membranes, *Water Res.*, 46 (2012) 2077-2087.

[34] Q.Y. Wang, Z.W. Wang, J. Zhang, J. Wang, Z.C. Wu, Antifouling behaviours of PVDF/nano- TiO_2 composite membranes revealed by surface energetics and quartz crystal microbalance monitoring, *RSC Adv.*, 4 (2014) 43590-43598.

[35] C.S. Ong, W.J. Lau, P.S. Goh, B.C. Ng, A.F. Ismail, Preparation and characterization of PVDF-PVP- TiO_2 composite hollow fiber membranes for oily wastewater treatment using submerged membrane system, *Desalin. Water Treat.*, 53 (2015) 1213-1223.

[36] Z. Yuan, X. Dan-Li, Porous PVDF/TPU blends asymmetric hollow fiber membranes prepared with the use of hydrophilic additive PVP (K30), *Desalination*, 223 (2008) 438-447.

[37] S. Majeed, D. Fierro, K. Buhr, J. Wind, B. Du, A. Boschetti-De-Fierro, V. Abetz, Multi-walled carbon nanotubes (MWCNTs) mixed polyacrylonitrile (PAN) ultrafiltration membranes, *J. Membr. Sci.*, 403 (2012) 101-109.

[38] W.Z. Lang, Q. Ji, J.P. Shen, Y.J. Guo, L.F. Chu, Modified poly(vinylidene fluoride) hollow fiber composite membranes reinforced by hydroxyapatite nanocrystal whiskers, *J. Appl. Polym. Sci.*, 127 (2013) 4564-4572.

[39] F. Yao, G.D. Fu, J.P. Zhao, E.T. Kang, K.G. Neoh, Antibacterial effect of surface-functionalized polypropylene hollow fiber membrane from surface-initiated atom transfer radical polymerization, *J. Membr. Sci.*, 319 (2008) 149-157.

Tables and Figures

Table 1. Composition (wt %) of the different dope solutions for membrane preparation.

Membranes	PVDF	PVP	DMF	TiO ₂	Ag ₃ PO ₄ /TiO ₂
P0	18	1.5	80.5	0	0
P1	18	1.5	80.4	0.1	0
P2	18	1.5	80.4	0	0.1
P3	18	1.5	80.2	0	0.3
P4	18	1.5	80.0	0	0.5
P5	18	1.5	79.5	0	1.0

Table 2 Contact angle, mechanical property, and porosity of the membranes.

Membrane	Contact angle (°)	Tensile strength (MPa)	Breakage elongation (%)	Porosity (%)
P-0	76.05	1.59	22.42	84.67
P-1	67.01	1.67	30.26	84.66
P-2	66.70	1.61	29.50	84.75
P-3	67.56	1.98	31.77	84.79
P-4	64.95	1.80	30.33	84.92
P-5	63.46	1.69	29.89	85.05

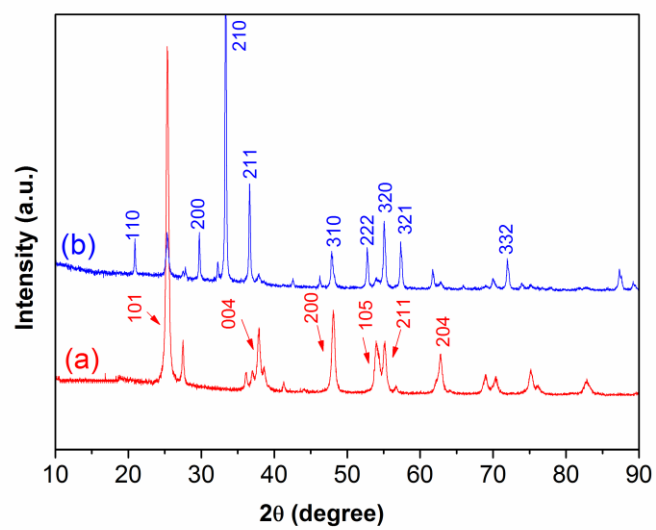


Fig. 1 XRD patterns of the pristine TiO_2 (a) and as-prepared $\text{Ag}_3\text{PO}_4/\text{TiO}_2$ nanocomposites (b).

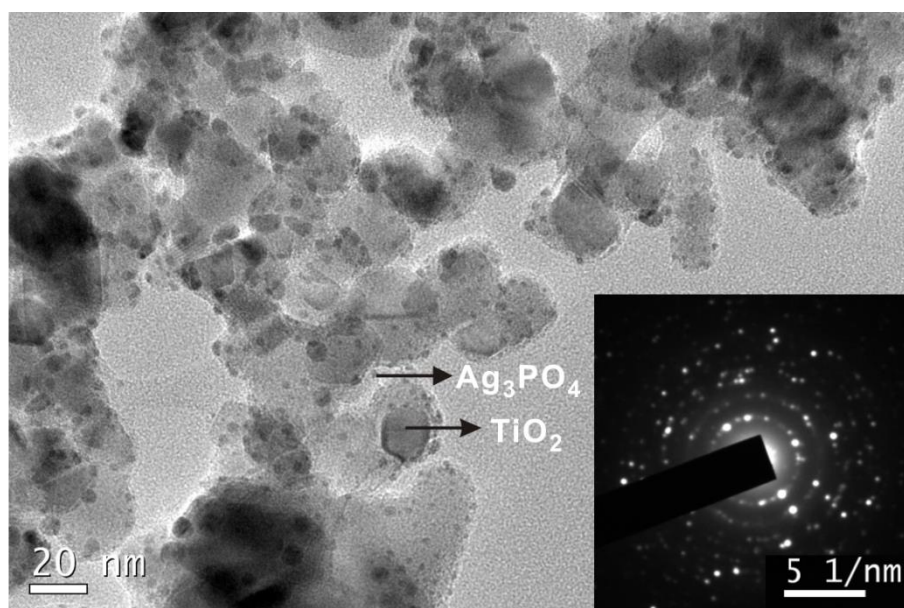


Fig. 2 The TEM image of $\text{Ag}_3\text{PO}_4/\text{TiO}_2$ nanocomposites. The inset shows the SEAD image of $\text{Ag}_3\text{PO}_4/\text{TiO}_2$ nanocomposites.

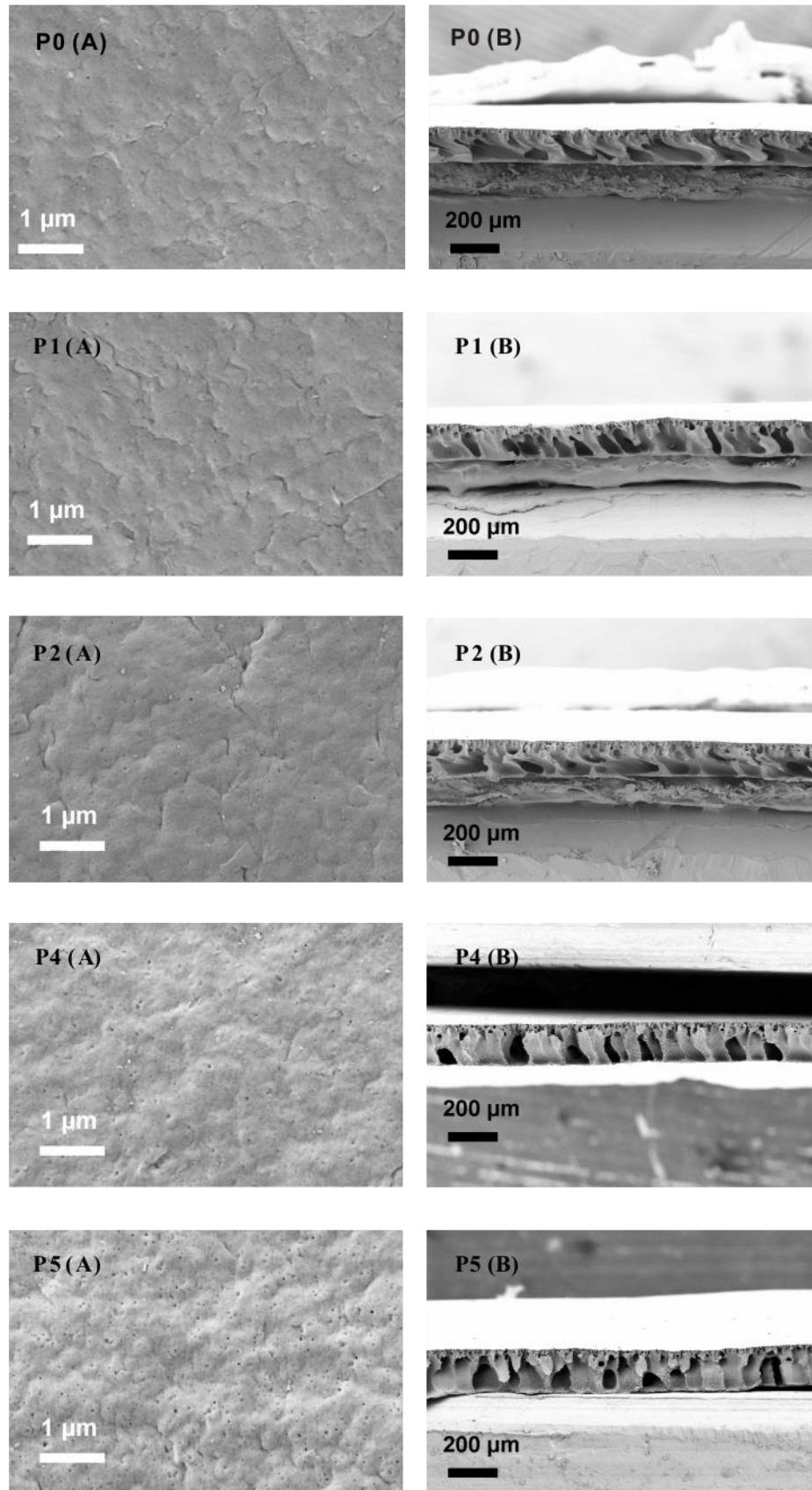


Fig. 3 Top-view (A) and cross-sectional (B) SEM images of the control (P0) and modified membranes (P1, P2, P4, P5).

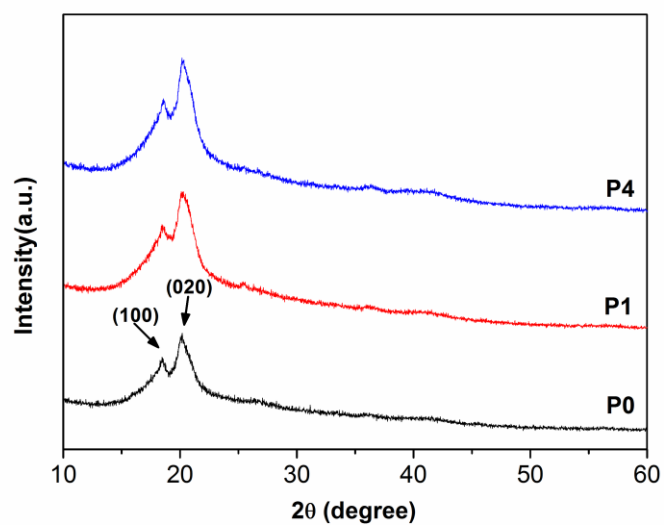


Fig. 4 XRD patterns of the pristine membrane (P0) and modified membranes (P1 and P4).

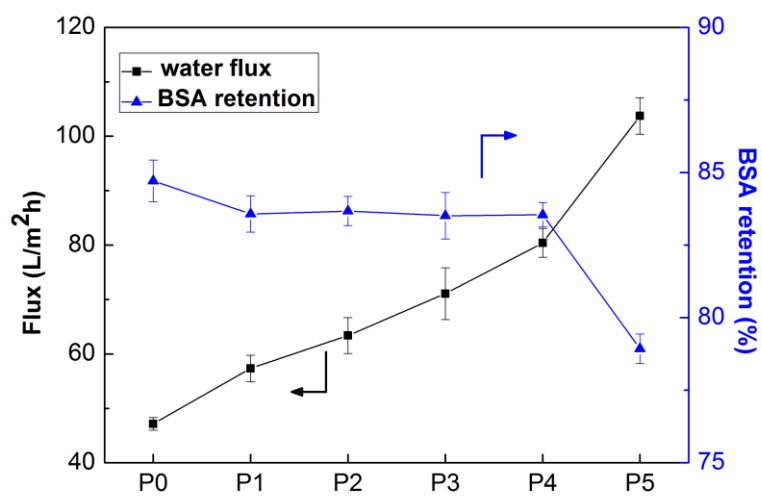


Fig. 5 Water flux (0.1 MPa) and the rejection of BSA of the PVDF membranes made with different TiO_2 and Ag_3PO_4/TiO_2 content.

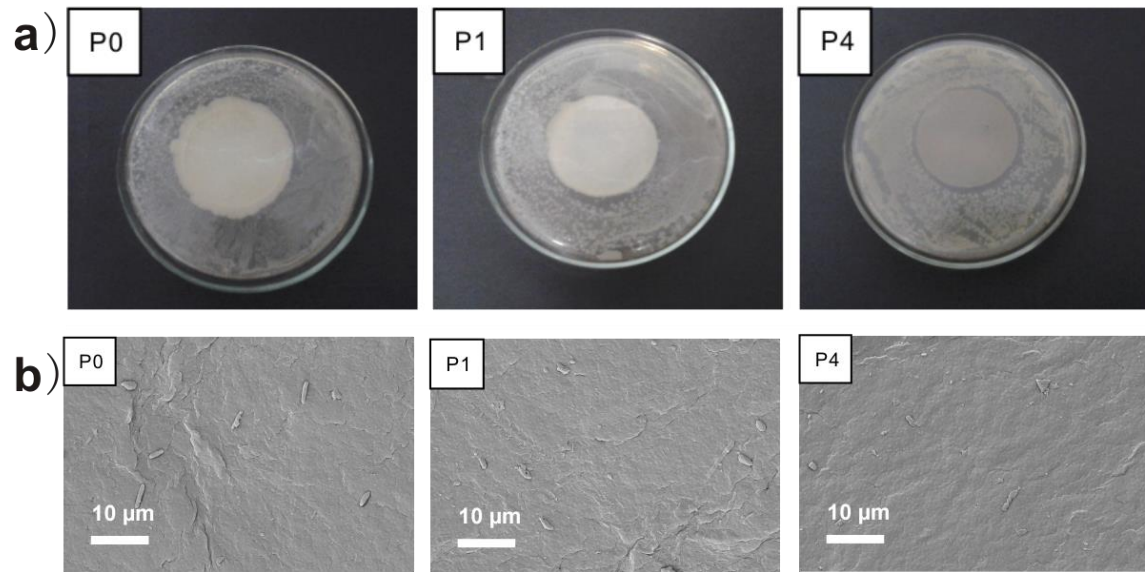


Fig. 6 a) Measurement of the antibacterial property of P0, P1 and P4 membranes using the halo zone test, b) SEM images of the bacteria adhered on the membrane surfaces.